JGR Space Physics

RESEARCH ARTICLE
10.1029/2021JA029195

Key Points:

- We present Jovian electron densities at high-latitudes on magnetic field lines connected to the Io torus and plasma sheet
- Sharp density gradients are found near the inner edge of the Io torus M-shell
- Our densities are consistent with partial electron densities measured by Juno's Jovian Auroral Distributions Experiment

Correspondence to:
S. S. Elliott,
sadie-tetrick@uiowa.edu

Citation:
Elliott, S. S., Sulaiman, A. H., Kurth, W. S., Faden, J., Allegrini, F., Valek, P., et al. (2021). The high-latitude extension of Jupiter's Io torus: Electron densities measured by Juno Waves. *Journal of Geophysical Research: Space Physics*, *126*, e2021JA029195. https://doi.org/10.1029/2021JA029195

Received 29 JAN 2021
Accepted 24 MAY 2021

The High-Latitude Extension of Jupiter's Io Torus: Electron Densities Measured by Juno Waves

S. S. Elliott[1], A. H. Sulaiman[1], W. S. Kurth[1], J. Faden[1], F. Allegrini[2,3], P. Valek[2], J. E. P. Connerney[4], R. W. Ebert[2], J. R. Szalay[5], F. Bagenal[6], and S. J. Bolton[2]

[1]Department of Physics and Astronomy, University of Iowa, Iowa City, IA, USA, [2]Southwest Research Institute, San Antonio, TX, USA, [3]Department of Physics and Astronomy, University of Texas at San Antonio, San Antonio, TX, USA, [4]Goddard Space Flight Center, Greenbelt, MD, USA, [5]Department of Astrophysical Sciences, Princeton University, Princeton, NJ, USA, [6]Laboratory for Astrophysics and Space Physics, University of Colorado, Boulder, CO, USA

Abstract We present Jovian electron densities measured by the Juno Waves instrument at high-latitudes (with magnetic latitudes of $50^{\circ}-80^{\circ}$) on magnetic field lines threading the Io torus and plasma sheet (with M-shells of 5.5–19) using the first 29 orbits of the Juno mission. We infer electron densities from characteristic frequency cutoffs and resonances in plasma wave spectra. Often more than one of the characteristic frequencies of the plasma can be identified, whose consistency provides credibility to the plasma density estimates. The majority of density measurements are on magnetic field lines threading the Io torus and intersecting Jupiter's ionosphere between Io's M-shell and the auroral main oval, but there is evidence of density dropouts near and poleward of the auroral oval, which may be important in auroral particle acceleration. Sharp density gradients are found near field lines mapping to the inner edge of the Io torus M-shells. These observations demonstrate the extension of elevated Io torus densities along field lines to higher latitudes.

1. Introduction

Jovian magnetospheric dynamics are known to be driven by internal sources of energy and mass (Russell, 2004, 2006). Within the Jovian system, the satellite Io is the site of numerous volcanic plumes that provide the main source of plasma in the Jovian magnetosphere. Nearly 1 ton/second of SO_2 from Io's atmosphere escapes the satellite (see review by Thomas et al., 2004). The neutrals can become ionized and captured by Jupiter's rotating magnetic field, creating a torus of plasma surrounding the planet. Since the discovery of the Io plasma torus (Brown, 1976; Kupo et al., 1976), the Voyager and Galileo spacecraft have made a number of detailed in situ measurements of the plasma properties at low latitudes. The Voyager 1 flyby of Jupiter in 1979 provided the first opportunity to measure radio and plasma waves within Jupiter's magnetosphere, resulting in electron density (n_e) profiles (Barnhart et al., 2009; Birmingham et al., 1981; Scarf et al., 1979; Warwick et al., 1979). Using in situ plasma data from Voyager 1, Bagenal et al. (1980) developed the first two-dimensional model of the Io torus, which was later replaced with improved models that included a diffusive equilibrium density model along Io torus field lines (Bagenal & Sullivan, 1981) and combined the in situ electron measurements of Sittler and Strobel (1987) and current magnetic field models (Bagenal, 1994).

The Galileo spacecraft performed a series of close flybys of Io, beginning on December 7, 1995, passing directly through the torus near the magnetic equator. Electron density profiles from Galileo measurements showed a sharp drop just inside the orbit of Io (Bagenal et al., 1997; Menietti et al., 2005). The parameters of three main regions (see Bagenal & Dols, 2020) for a detailed description on each region) were found to be the following: a cold torus, with peak electron density of $\sim 10^3$ cm^{-3} at $\sim 5.3\ R_J$ (where 1 R_J is a Jovian equatorial radius = 71,492 km), a warm torus, with peak electron density of $\sim 2 \times 10^3$ cm^{-3} at $\sim 6.0\ R_J$, and a "ribbon" region, with peak electron density of $\sim 3 \times 10^3$ cm^{-3} at $\sim 5.6 - 5.9\ R_J$. These Galileo observations were consistent with earlier Voyager measurements in these regions (Bagenal, 1994).

Although there were no in situ measurements at higher latitudes (prior to the Juno mission), early studies relied on Voyager 1 observations of whistlers, which provide electron density estimates along magnetic field lines connecting the lightning source to the spacecraft location (Crary et al., 1996; Tokar et al., 1982;

Wang et al., 1998a, 1998b). These studies found both maximum ($\sim 2 \times 10^3$ cm^{-3} for $L = 5.2 - 6.2$ [Tokar et al., 1982]) and minimum (~ 8 cm^{-3} for $L = 5.7 - 5.9$ [Wang et al., 1998a], ~ 3–5 cm^{-3} for $L = 5.3$ [Wang et al., 1998b]) electron densities for high latitude regions connected to the Io torus. Although remote sensing measurements are important, sharp density gradients and low-density regions at intermediate latitudes can greatly affect whistler dispersion and propagation.

High-latitude in situ measurements of the electron number density are important because n_e is one of the key parameters used to characterize the structure and dynamics of planetary magnetospheres and an important input to many magnetospheric and ionospheric models. One way to measure the electron density is through particle counting via plasma instruments, but it is sometimes difficult to measure the cold plasma, especially when dealing with spacecraft potential. Plasma wave instruments can support plasma instruments through indirect, yet accurate, measurements of electron densities that are relatively free of perturbing effects of the spacecraft (Kurth et al., 2015; Persoon et al., 2019).

Plasma waves have distinct frequency cutoffs and resonances that are dependent on the background plasma properties and therefore identification of these features can be used to constrain parameters such as the electron density. During times of high radiation, when the electron sensors are overwhelmed by penetrating radiation, when there is spacecraft charging, or when the electron energy is outside the range of the sensors, plasma wave instruments are often able to determine the electron density, which aids in the continuity of coverage. In fact, for many missions, wave measurements provide the standard by which plasma densities obtained by other instruments are calibrated (see, for example, Allegrini et al., 2020; Bagenal et al., 2016; Scudder et al., 1981). Quasi-thermal noise (QTN) spectroscopy is another technique used for density determination because a passive electric antenna is sensitive to fluctuations due to the thermal motion of ambient electrons and ions (Le Chat et al., 2009; Meyer-Vernet & Perche, 1989). QTN spectroscopy is not affected by the spacecraft potential and therefore is an advantageous way of density determination. Unfortunately, Juno's electric antenna is too short to perform this technique (see Kurth et al., 2017), therefore, we rely on plasma wave spectral cutoffs and resonances for our density measurements. A detailed explanation of the methodology for inferring electron density using Waves across the Juno mission can be found in Sulaiman et al. (2021).

The Juno spacecraft has a unique polar orbit, which provides in-situ measurements of the Jovian high-latitude polar regions (Bagenal et al., 2017; Bolton et al., 2017). Juno is equipped with both a plasma instrument, the Jovian Auroral Distributions Experiment (JADE) (McComas et al., 2017) and a plasma wave instrument, Waves (Kurth et al., 2017). JADE has two identical electron sensors (JADE-E) and an ion sensor (JADE-I). JADE-E measures electrons in the energy range of ~0.1–100 keV using a spherical top-hat electrostatic analyzer, two deflectors, and a microchannel plate with an anode ring underneath (McComas et al., 2017). Waves makes spectral density measurements of both the wave electric field from 50 Hz to 40 MHz with a single-axis dipole antenna contained in the spacecraft's spin plane, and the wave magnetic field from 50 Hz to 20 kHz with a single-axis search coil magnetometer along the spacecraft's spin axis. The low frequency receiver (LFR) on Waves has two low-frequency channels that sample plasma waves within the frequency range of 50 Hz to 20 kHz for the electric and magnetic fields from both sensors at the same time. A higher frequency channel of the LFR provides electric field spectra and waveforms from ~10 to 150 kHz. A digitized waveform comes from each channel and is either sent to the ground in its entirety in burst mode or for the majority of times as a spectrum analyzed in the digital processing unit (DPU) in order to produce spectra (Kurth et al., 2017).

This study presents measurements of the electron density in the previously unexplored Jovian high-latitude regions, beginning around Io's M-shell (~5.9) and extending to higher M-shells for the first 29 orbits. Here, we use M-shell in the same manner as dipole L-shell, but using the JRM09 field model (Connerney et al., 2018) with the Jovian current sheet included (Connerney et al., 1981). We use burst mode plasma wave measurements for determination of the electron number density. The electron density is calculated from measurements of the electron plasma frequency and/or the lower hybrid resonance frequency. Therefore, our measurements are limited by times when burst mode data are obtained and when relevant characteristic frequencies, dependent on the electron density, are detected.

2. Methods and Wave Observations

A common way to determine the electron density is by locating the upper hybrid resonance frequency, either by observing thermally excited electrostatic emission or upper hybrid waves from plasma instabilities, both of which are very common features in planetary magnetospheres (Birmingham et al., 1981; Gurnett et al., 1981, 1996, 1998, 2001; Kurth et al., 1979, 1980, 2015; Menietti et al., 2005; Mosier et al., 1973; Shaw & Gurnett, 1975; Warwick et al., 1979;). However, due to the unique plasma environment of the Jovian high-latitude regions close to the planet (i.e., the electron cyclotron frequency, f_{ce}, is much larger than the electron plasma frequency, f_{pe}, with f_{pe} / f_{ce} ranging from $\sim 6 \times 10^{-4}$ to $\sim 4 \times 10^{-2}$), the upper hybrid resonance frequency is often equal to, or nearly equal to, the electron cyclotron frequency. Therefore, determination of the electron number density from the upper hybrid frequency is not possible in these previously unexplored Jovian high-latitude, low-altitude regions.

For this study, we use four different methods to determine the electron number density in this unique plasma environment. The first two methods deal with waves propagating in the whistler mode, which have an upper and a lower cutoff frequency at the electron plasma frequency and the lower hybrid resonance frequency, respectively. When an upper cutoff of the whistler-mode emission is clearly identified in the data, the electron number density is then calculated from the following equation (e.g., Persoon et al., 2019):

$$f_{pe} = 8980\sqrt{n_e}\,, \tag{1}$$

where f_{pe} is the electron plasma frequency in Hertz and n_e is the electron number density in electrons per cubic centimeter. It should be noted that it is possible for the detectability of the whistler-mode to drop below f_{pe}, but a sharp frequency cutoff more likely indicates the plasma frequency, as opposed to a gradual cutoff. This method of determining electron density from the propagation cutoff of whistler-mode waves at the electron plasma frequency (Gurnett & Bhattacharjee, 2017; Stix, 1962) has commonly been used to determine the electron density in Saturn's ionosphere (Persoon et al., 2005, 2019; Sulaiman et al., 2017). However, using the lower cutoff of the whistler-mode emission at the lower hybrid frequency for electron density determination is uncommon. Typically, for example, in Saturn's magnetosphere, the lower hybrid frequency is equal to the proton plasma frequency (Sulaiman et al., 2017, 2021), but due to Jupiter's unique plasma environment, the lower hybrid frequency can deviate from the proton plasma frequency and become the proton cyclotron frequency, or some frequency in between (Sulaiman et al., 2021). When a lower cutoff of the whistler-mode emission (i.e., the lower hybrid frequency) is clearly identified in the data and is clearly above the proton cyclotron frequency, f_{cH^+}, the following equation can be solved for the electron plasma frequency, where S is a component of the dielectric tensor for a cold, magnetized plasma (Gurnett & Bhattacharjee, 2017; Stix, 1962):

$$S = 0 = 1 - \sum_s \frac{f_{ps}^2}{f^2 - f_{cs}^2} = 1 - \frac{f_{pe}^2}{f^2 - f_{ce}^2} - \frac{f_{pH^+}^2}{f^2 - f_{cH^+}^2} \tag{2}$$

which assumes a two-species electron and proton quasi-neutral plasma, where f_{pe} and f_{pH^+} are the electron and proton plasma frequencies, respectively; f_{ce} and f_{cH^+} are the electron and proton cyclotron frequencies, respectively. f has two positive solutions, the lower of the two being the lower hybrid frequency, f_{lh} (in Hertz). The electron cyclotron frequency is determined from |B| measured by the Magnetometer instrument (MAG) by utilizing a pair of tri-axial Fluxgate Magnetometers (FGMs) to provide magnetic field measurements at sample rates up to 64 vector samples per second (Connerney et al., 2017). The electron cyclotron frequency is then calculated using the total measured magnetic field and the following equation:

$$f_{ce} = 28B \tag{3}$$

where B is the magnetic field in nT. Once f_{pe} is solved for in Equation 2, Equation 1 can then be used to compute n_e.

The third method to determine the electron number density is through detection of plasma oscillations, which provide direct determination of the electron density through the frequency of the waves at f_{pe}. Electron plasma oscillations are polarized parallel to the magnetic field, meaning the frequency of the wave is

not impacted by the magnetic field. When plasma oscillations are detected, their frequency (f_{pe}) is used to compute n_e in Equation 1.

The fourth method to determine the electron number density is through detection of the lower cutoff of the electromagnetic ordinary mode (O-mode) emissions, which occurs at the electron plasma frequency (Gurnett & Bhattacharjee, 2017; Stix, 1962). It should be noted that this cutoff generally provides an upper limit to f_{pe}, hence n_e, since the cutoff may occur remote from the observer and the local density could be significantly lower. Ordinary mode emissions were frequently used to determine the plasma density in the Jovian magnetosphere by the Voyager 1 and 2 spacecraft (Ansher et al., 1992; Barbosa et al., 1990; Barnhart et al., 2009; Gurnett et al., 1979, 1980, Gurnett et al., 1981; Scarf et al., 1979) and is a common technique for electron density determination by plasma waves (Gurnett & Frank, 1974; Gurnett & Shaw, 1973). When a lower cutoff of O-mode emission is detected, Equation 1 is used to compute the electron number density. For completeness, the identification of the upper hybrid resonance frequency, when $f_{pe} \geq f_{ce}$ (or when $f_{pe} < f_{ce}$, but of order f_{ce}), would constitute a fifth method (e.g., Gurnett et al., 2001; Kurth et al., 2015), but is not used here.

To summarize, the four methods used in this study to determine the electron number density are the following:

1. f_{pe} from the upper cutoff of whistler-mode emission
2. f_{lh} from the lower cutoff of whistler-mode emission
3. f_{pe} from the frequency of plasma oscillations
4. f_{pe} from the lower cutoff of ordinary-mode emission

Figure 1 shows example plasma wave spectra and the associated electron density profile for each interval, illustrating each method used to obtain electron densities. The black dots in the spectra indicate digitized frequencies, and the red dots indicate computed frequencies. The green line shows the proton cyclotron frequency. For example, Figure 1a shows the digitized lower hybrid frequency (black dots, using method 2) and the computed electron plasma frequency (red dots). Figure 1b shows the same time interval as Figure 1a, but now the electron plasma frequency is digitized, based on the location of plasma oscillations (black dots, using method 3) and the upper cutoff of whistler-mode waves (black dots, using method 1), and the lower hybrid frequency is computed from these digitized points (red dots). Figures 1c, 1f and 1h show the computed electron density profiles (density is represented by open circles, with the color indicating which method was used to obtain such densities). It should be noted that it is not possible for the lower cutoff in Figure 1g (second set of black dots) to be a cutoff frequency other than the plasma frequency, such as the lower hybrid frequency or the $L = 0$ frequency since neither can go below the proton cyclotron frequency (Sulaiman et al., 2021).

There are times when two or more characteristic frequencies can be identified for the same time interval, each of which can be used to determine f_{pe}, hence n_e. These times are important, because the densities inferred using multiple techniques should be similar. If so, such consistency provides confidence in the densities.

It should also be noted that the four methods described above are complementary to one another, meaning that any method can be used to derive the other characteristic frequencies of the plasma (i.e., the plasma frequency or the lower hybrid frequency, along with the electron cyclotron frequency, can be used as the observed frequency to compute the other characteristic frequencies). This is important because not all spectral features are always present. Although the methods are straightforward in principle, they must be used with care.

In order to generate the electron density data set, we first look for times when Juno is in the high-latitude regions (within $10\,R_J$, with magnetic latitudes between 50° and 80°) and burst mode data are obtained. In principle, the survey mode can also be used to determine densities using any of the four methods discussed here. However, the lower spectral resolution sometimes makes the identification of the characteristic frequencies uncertain, not to mention less accurate. Trajectory plots of the Juno spacecraft footprint are used to select times for this study. Once times with burst mode data available are selected, we then visually identify well-defined spectral features in the Waves data that are associated with the electron density (i.e., the

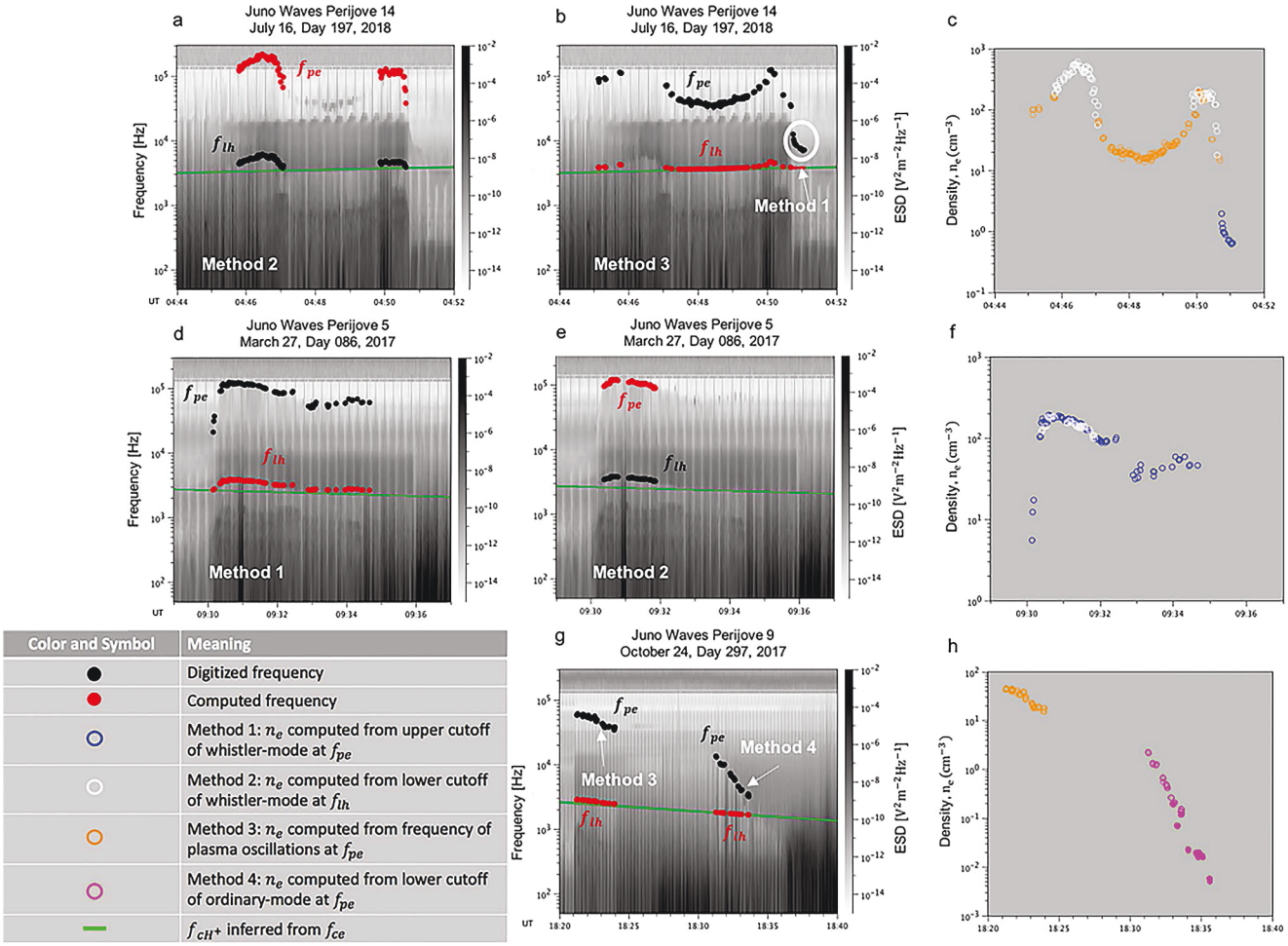

Figure 1. Electric field frequency-time spectrograms from Juno Waves (a, b, d, e, g) and their associated electron density profiles (c, f, h). The gray scale on the spectra indicates the electric field spectral density (ESD). The black dots indicate the digitized frequency and the red dots indicate the computed frequency, using the method indicated in each spectrum. The green lines show the proton cyclotron frequency (f_{cH^+}) inferred from the electron cyclotron frequency (f_{ce}). Electron density profiles (c, f, h) show the electron density calculated from the associated method, as indicated by the color. Overlap and continuation shows electron densities calculated from different methods are consistent. (a) The lower hybrid, f_{lh}, was digitized (black dots) and the electron plasma frequency, f_{pe}, was computed (red dots). (b) f_{pe} was digitized from plasma oscillations and the upper cutoff of whistler-mode emissions (black dots), and f_{lh} was computed (red dots). (c) Electron density profile from three different methods (methods 1, 2, and 3). (d) f_{pe} was digitized from the upper cutoff of whistler-mode emissions (black dots), and f_{lh} was computed (red dots). (e) f_{lh} was digitized (black dots), and f_{pe} was computed (red dots). (f) Electron density profile from two different methods (methods 1 and 2). (g) f_{pe} was digitized from plasma oscillations and the lower cutoff of O-mode emissions (black dots), and f_{lh} was computed (red dots). (h) Electron density profile from two different methods (methods 3 and 4).

electron plasma frequency and/or the lower hybrid frequency). These characteristic frequencies are then digitized by selecting a box covering a frequency-time range and a digitizing mode ("peak," "top," "bottom," or "manual"). This process is done through a publicly available software tool, Autoplot (see Autoplot.org). The "peak" mode finds the frequency corresponding to the maximum value (i.e., maximum electric field spectral density, useful for narrowband emissions like plasma oscillations or upper hybrid emissions) for each record in the selected box. The "top" mode finds the frequency where the slope is most quickly decreasing as a function of increasing frequency, as for the upper cutoff of an emission. Similarly, the "bottom" mode finds where the slope is most quickly increasing, for the lower cutoff of the whistler-mode or ordinary-mode. The "manual" mode finds the geometric middle of the box frequency range where the slopes are too weak for the algorithm to identify. Once the characteristic frequencies are digitized, we then calculate the other characteristic frequencies of the plasma using Equations 1–3. This process was done using the publicly available software tool Autoplot (autoplot.org) and then using Autoplot's scripting tool to run a script for the digitizing and computation of characteristic frequencies.

Finally, we look for consistencies between the observed and calculated frequencies in order to prevent misidentification of characteristic frequencies and in turn, the electron density. Many of the densities are obtained using more than one characteristic frequency, validating our interpretations of the wave spectra. Figure 1 highlights such consistencies, showing continuity and overlap in the observed and calculated values for both the lower hybrid and electron plasma frequency. For example, Figure 1f shows times when both the lower hybrid and electron plasma frequency are observed and give consistent densities. This provides us with confidence that the characteristic frequencies have been properly identified.

3. Results

The Waves data files used in this study can be found and downloaded for public use at https://doi.org/10.5281/zenodo.4456343. The resulting electron density data set includes a complete list of measurement times, characteristic frequencies of the plasma (including f_{ce}, f_{cH+}, f_{pe}, lower and upper hybrid resonance frequencies, and $L = 0$ and $R = 0$ frequencies, which indicate low-frequency cutoffs of left- and right-handed polarized waves, respectively), and densities. Columns indicating the digitized frequency and mode (i.e., peak, top, bottom, or manual), the characteristic frequency assumed, and ephemeris parameters (i.e., magnetic latitude, longitude, M-shell, and radial distance), are also included.

Figure 2 shows the full (perijove 1–29) high-latitude electron density data set in a cylindrical magnetic coordinate system (Figure 2a), projected along the JRM09 model magnetic field to the 1-bar level over the northern and southern polar regions (Figure 2b), plotted as a function of Juno's radial distance and M-shell (Figure 2c), and median densities for M-shells between 5 and 8 (Figure 2d). One notable feature is the electron density dependence on a variety of spatial parameters, such as the distance from Jupiter, M-shell, and magnetic latitude. Unlike a previous equatorial density study done at Saturn (Persoon et al., 2005), where a power law relationship was found between the density and radial distance, no such relationship can be deduced from the Juno observations because it is difficult to resolve the dependence of electron density on a single parameter due to the interdependence of these parameters. Therefore, care must be taken when analyzing density dependencies on spatial parameters. Different densities in overlapping measurements in Figure 2a highlight the variability of this region of space.

Figure 2b shows how the electron density is distributed near and between the M-shell of Io's orbit (outer black line) and the main auroral oval (inner two black lines). The majority of density measurements are located between Io's orbital M-shell and the main auroral oval. However, there are a few noteworthy measurements near and poleward of the main oval. It should be noted that there are only a few measurements in these regions because, for a majority of the time, plasma waves associated with the electron density could not be confidently identified and/or burst mode data was unavailable. Some of these density measurements drop to very low values (on the order of 1 cm^{-3} and below). Low electron density measurements at low altitudes are important because they can lead to Alfvénic acceleration capable of producing substantial parallel electric fields, which are important in auroral particle acceleration (Lysak & Song, 2011 and references therein). Density cavities or dropouts are known to have a connection with the auroral acceleration region at Earth (Paschmann et al., 2003). Parallel electric fields that cause upward-directed ion beams and conics in Earth's auroral cavity region have been found to be correlated with density depletions and are associated with auroral acceleration processes (Persoon et al., 1988). In fact, upward proton beams and ionospheric outflow associated with Jupiter's auroral emissions have been observed by Juno (Szalay et al., 2021).

Another notable feature is that the electron density values have a drop off at the location of Io's orbit. This feature is even more pronounced in Figures 2c and 2d, where densities are plotted as a function of M-shell (up to 20) and radial distance. The vertical black dashed line in Figure 2d shows an M-shell of 5.9 (the orbit of Io). A decrease in electron density is observed at M-shells inside the Io torus region (smaller M-shells). In Figure 2d, the median electron density is plotted for each M-shell between 5 and 8. A sharp drop in electron density (down to ~0.1 cm^{-3}) is observed just within $M = 5.9$ and peak densities (up to $\sim 2 \times 10^2$ cm^{-3}) are found around $M = 6.1$–6.3.

Figure 2d also highlights three clear subsets of the data around the Io torus region (i.e., lower densities between $M = 5.5$ and 5.9, indicated by the blue bar, higher densities between $M = 6.0$ and 6.5, indicated by the red bar, and intermediate densities between $M = 7.0$ and 8.0, indicated by the green bar). We analyzed

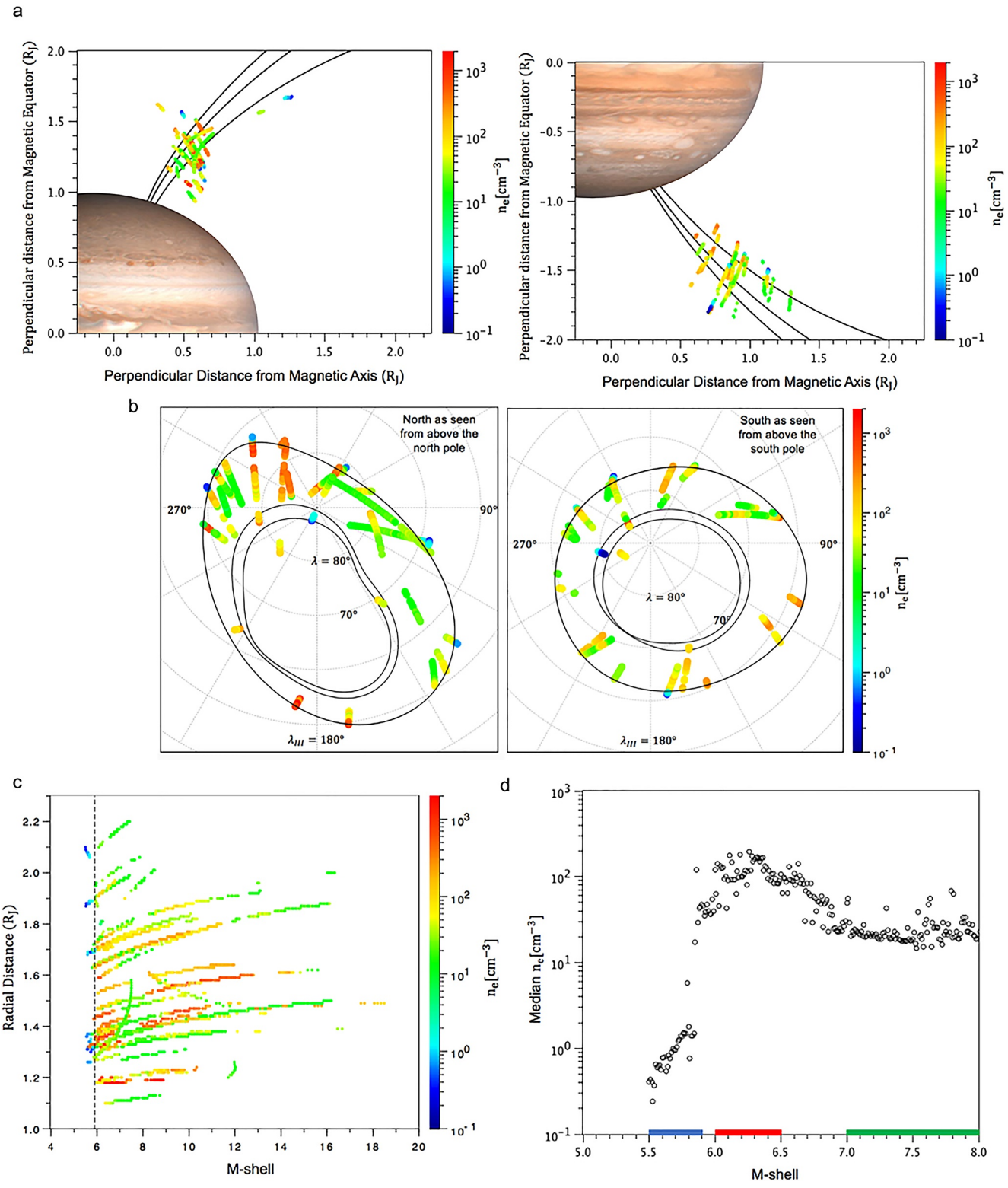
a
Perpendicular distance from Magnetic Equator (R_J)
Perpendicular Distance from Magnetic Axis (R_J)
$n_e[cm^{-3}]$
b
North as seen from above the north pole
South as seen from above the south pole
270°
90°
λ = 80°
70°
λ_{III} = 180°
c
Radial Distance (R_J)
M-shell
d
Median $n_e[cm^{-3}]$
M-shell

Figure 2

the median values of these three subsets and found the following to be true: the median of the lower density subset is ~1 cm^{-3}, the median of the higher density subset is ~10^2 cm^{-3}, and the median of the intermediate density subset is ~20 cm^{-3}. Although no in situ high-latitude electron density measurements have been made prior to Juno, we can compare our densities to those measured by Voyager 1 via lightning whistlers, which provide measurements along the field lines connecting the lightning source to the spacecraft location. Tokar et al. (1982) found the maximum electron density measured to be ~2×10^3 cm^{-3} (near the equator for L between 5.2 and 6.2), and Wang et al. (1998a, b) found a minimum to be ~8 cm^{-3} (L = 5.7–5.9) and ~3–5 cm^{-3} (L = 5.3). Our high-density median is found to be an order of magnitude smaller than what was found by Tokar et al. (1982), and our low-density median is found to be the same order of magnitude as Wang et al. (1998a, b). The difference between our in situ densities and the remote sensing observations from Tokar et al. (1982) is due to the rapidly rotating Jovian system. Centrifugal forces work to confine the majority of heavy ions to the plasma sheet (or the centrifugal equator). The electrons are less impacted by the centrifugal force, but due to charge neutrality and the development of ambipolar electric fields, caused by small charge separation between the centrifugally confined ions and the electrons, a majority of the electrons are confined to low-latitudes. A model for the high-latitude structure of the Io plasma torus was developed by Moncuquet et al. (2002) using the general properties of plasma tori. To summarize, the lower energy particles become confined to the centrifugal equator, while more energetic particles can escape to higher latitudes, resulting in higher kinetic energy in the high-latitude regions (i.e., farther from the centrifugal equator). Therefore, we expect higher temperatures and lower electron densities at higher latitudes, but the important result is that we are measuring torus densities on the high-latitude extension of torus field lines.

High-latitude electron density measurements are also key to explain the brightness of Io's footprint. Hess et al. (2013) found that a decrease in electron density could cause significant dimming in the satellite footprint brightness. In fact, the footprint was found to completely disappear during an injection event (Bonfond et al., 2012, 2017).

As recently reviewed by Bagenal and Dols (2020), there are three main regions to Io's plasma torus: (1) an outer region with a roughly circular cross section that contains 90% of the mass with density decreasing outward past Europa's orbit; (2) there is narrow, dense but vertically extended region—sometimes called the "ribbon"—inside Io's orbit; and (3) extending inward from the ribbon is a thin disk where the cold, dense (and predominantly S^+) plasma is tightly confined to the centrifugal equator. The vertical extension of the plasma in the ribbon and outer torus is due to a combination of warmer ion temperatures, lower mass-charge ratios (the dominant ions are O^+ and S^{++}), and a significant contribution of protons, presumably escaped from Jupiter's ionosphere.

The observed density decrease around M = 5.9 is reminiscent of density gradients observed at the near-equatorial inner edge of the Io torus by the Galileo spacecraft (Gurnett et al., 2001; Menietti et al., 2005). During orbit A-34, when the Galileo spacecraft passed into the region between the Io torus and Jupiter near the magnetic equator, Menietti et al. (2005)] reported a strong electron density gradient near the inner edge of Io's cold plasma torus (see Figures 3c and 3f). They found the peak electron density (2.6×10^3 cm^{-3} around 5.62 R_J) occurs just before the inner edge of Io's hot torus. When the spacecraft entered the inner edge of the cold torus (around 4.76 R_J) the density dropped substantially to values on the order of 1 cm^{-3}. It should be noted that the upper hybrid resonance in this inner torus region is not visible. Menietti et al. (2005) identified a low-frequency cutoff inward of the Io torus as either $f_{l=0}$ or f_{pe} because it was not clear whether the emissions at higher frequencies were z-mode or ordinary-mode. For Figure 3c, we have interpreted the low-frequency cutoff as f_{pe} because this is consistent with other emissions observed in the spectra. Nevertheless, they identified the regions inward of the Io torus as one with very low plasma densities. In this

Figure 2. (a) Electron densities (n_e, color bar) plotted in a cylindrical magnetic coordinate system, which uses the JRM09 magnetic field model (Connerney et al., 2018), for the north (left) and south (right) hemispheres. Sample magnetic field lines (M = 6, 8, and 10) are shown for equatorial crossing distances of 6, 8 and 10 R_J (black lines). These densities were obtained for perijoves 1–29. (b) Orthographic projections - Electron densities plotted at the location of Juno mapped to the 1-bar level (using JRM09 magnetic field model from Connerney et al., 2018) onto the northern (left) and southern (right) hemispheres. The inner two solid black lines represent the location of the statistical auroral oval from Hubble Space Telescope observations (Bonfond et al., 2012, 2017) and the outer black line shows the location of the Io footprint. (c) Electron densities plotted as a function of M-shell and radial distance. The vertical black dashed line is at an M-shell of 5.9 (the orbit of Io). A density drop off can be seen at M-shells inside the Io torus region. (d) Median electron densities for each M-shell from 5 to 8. A sharp drop in density (down to ~0.1 cm^{-3}) is observed just within M = 5.9 and peak densities (up to ~2×10^2 cm^{-3}) are found around M = 6.1–6.3. The blue bar shows the lower density subset, the red bar shows the higher density subset, and the green bar shows the intermediate density subset.

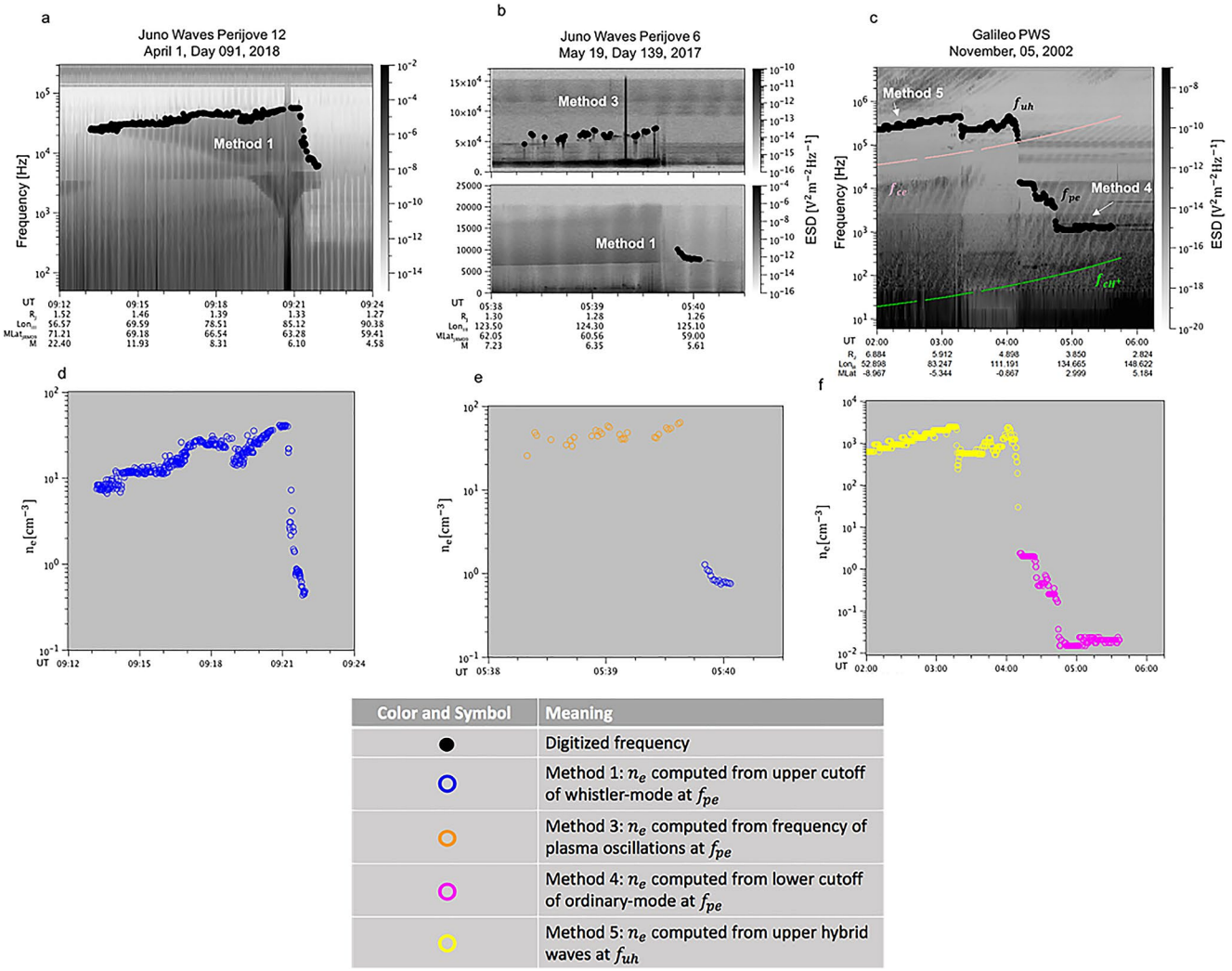

Color and Symbol	Meaning
●	Digitized frequency
○	Method 1: n_e computed from upper cutoff of whistler-mode at f_{pe}
○	Method 3: n_e computed from frequency of plasma oscillations at f_{pe}
○	Method 4: n_e computed from lower cutoff of ordinary-mode at f_{pe}
○	Method 5: n_e computed from upper hybrid waves at f_{uh}

Figure 3. (a) Electric field frequency-time spectrogram for perijove 12. The gray scale indicates the electric field spectral density (ESD). The upper cutoff of an auroral hiss funnel, associated with the Io plasma torus is digitized (method 1). The black dots show the location of the electron plasma frequency. A sharp drop off in density is observed around 09:21 on the inner edge of the Io plasma torus. (b) Burst mode electric field spectral densities for perijove 6. (Top) Low Frequency Receiver-Hi (LFR-Hi) data showing plasma oscillations at the local electron plasma frequency (black dots, method 3). (Bottom) Low Frequency Receiver-Lo (LFR-Lo) data showing a continuation of the electron plasma frequency based on the upper cutoff of whistler-mode emission (black dots, method 1). A sharp drop off in density is observed when the plasma frequency drops from LFR-Hi to LFR-Lo (around 05:39). (c) Electric field frequency-time spectrogram from the Galileo plasma wave instrument (PWS) on day 309 of 2002, from Menietti et al. (2005). The first set of black dots show the upper hybrid resonance frequency. The second set of black dots show the electron plasma frequency from the lower cutoff of ordinary-mode emissions. The pink and green lines show the electron cyclotron frequency and the proton cyclotron frequency, respectively. (d), (e), and (f) show the corresponding electron density profiles for perijove 12 (d), perijove 6 (e), and Galileo on day 309 of 2002 (f).

paper, we show a continuation of the density gradient and low-density region to higher latitudes. It should be noted that Galileo observed two density drops: one just inside $M = 5.9$ and another inside $M = 4.9$. The density drop observed inside $M = 5.9$ is the same one Juno observes at higher latitudes, while the cold torus is confined to low latitudes.

Figure 3a shows an example of Juno plasma wave observations during a high-latitude pass through the flux tube connected to Io's auroral footprint on perijove 12, when Io's magnetic footprint nearly coincided with Juno's (most likely directly connected to Io's Main Alfvén Wing [Szalay et al., 2020]). The wave-particle interactions for this event were analyzed by Sulaiman et al. (2020) wherein they found evidence of Alfvén, ion cyclotron, and whistler modes. The upper cutoff of an auroral hiss funnel (black dots in Figure 3a), associated with the Io plasma torus, was used to compute the electron number density (method 1). A sharp density

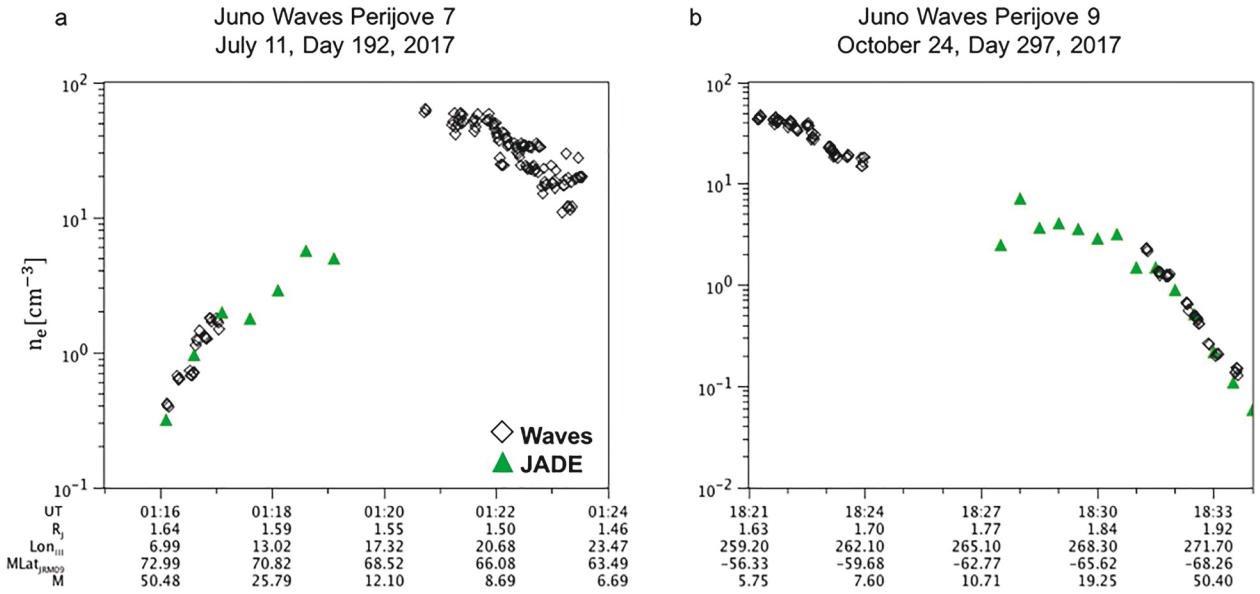

Figure 4. Density profiles for times during perijove 7 (a) and perijove 9 (b). The black diamonds show electron density measurements from Waves and the solid green triangles show partial electron density measurements from JADE (McComas et al., 2017). During times when both Waves and JADE can make the electron density measurements, their values agree well. Times when only Waves measurements are available correspond to when JADE cannot confidently measure the bulk of the electron density.

depletion was observed around 09:21, near $M = 5.9$. The peak electron density of ~40 cm^{-3} is observed just before 09:21, at $M = 6.1$ (at an altitude of ~ 0.34 R_J). The electron density then decreased to the order of 1 cm^{-3} at $M = 5.8$ (at an altitude of ~ 0.33 R_J) (Figure 3d).

Figure 3b shows another example of this density depletion, but for a high-latitude pass through the Io torus on perijove 6, with a larger angular separation between Juno and Io (~ 40.40° $\Delta\lambda_{SIII}$, where $\Delta\lambda_{SIII}$ = System-III longitude = Juno's footprint longitude–Io's footprint longitude). The top panel shows the Low Frequency Receiver-Hi (LFR-Hi) data and the bottom panel shows data from the Low Frequency Receiver-Lo (LFR-Lo). The observed plasma oscillations were used to compute the electron density in the top panel (method 3), and the upper cutoff of the whistler-mode emission was used in the bottom panel (method 1), showing a continuation of the electron plasma frequency between the two channels. The peak electron density reaches a value of ~60 cm^{-3} around 05:59:30, at $M = 5.85$ (at an altitude of ~ 0.29 R_J) and then drops to ~1.2 cm^{-3} around 05:39:45, at $M = 5.61$ (at an altitude of ~ 0.26 R_J) (Figure 3e).

When comparing these gradients to the Menietti et al. (2005) observation (Figures 3c and 3f), we find that Juno observes much smaller peak densities at higher latitudes (~40–60 cm^{-3}, compared to 2.6×10^3 cm^{-3}), but minimum densities are found to roughly be the same (the order of ~1 cm^{-3}). Sharp density gradients, like those shown in Figure 3, are also observed during other perijove passes when Juno flies through the Io torus and reaches M-shells below 5.9. This gradient is the high-latitude extension of the Io torus.

We can also compare our Waves density measurements to those measured by Juno's JADE instrument, which measures the partial electron density through particle counting in its energy range for limited times during these high-latitude crossings. Figure 4 shows electron density profiles for times during perijove 7 (Figure 4a) and perijove 9 (Figure 4b). The black diamonds in the figure show the electron density measurements from Waves and the green triangles show the partial electron densities from JADE (Allegrini et al., 2021). We use the term "partial" here because JADE measures the part of the electron distribution that is, within its energy range (~0.1–100 keV). Thus, it does not account for electrons with energies outside its energy range, even though they contribute to the total electron density. There is a good agreement between Waves and JADE electron densities when both instruments are able to make the measurement. However, for many of the passes JADE is unable to measure the total electron density, especially near the Io torus region where the electron sensors are overwhelmed by penetrating radiation and when the core of

the electron distribution falls outside their energy range. Waves, however, is not affected by these conditions and can make these critical observations in this region. A detailed survey of electron partial densities and temperatures using JADE data over Jupiter's main auroral emission is presented in Allegrini et al. (2021).

4. Summary

In this paper, we have presented measurements of Jovian high-latitude electron densities on the near Io torus field lines measured by the Juno Waves instrument for the first 29 orbits. To determine the electron density, we employed four different methods of interpreting the plasma wave spectra:

1. f_{pe} from the upper cutoff of whistler-mode emission
2. f_{lh} from the lower cutoff of whistler-mode emission
3. f_{pe} from the frequency of plasma oscillations
4. f_{pe} from the lower cutoff of ordinary-mode emission

We found that the electron densities depend on a variety of spatial parameters and it is difficult to separate correlations due to the interdependence of spatial parameters in this region of space. Most of our measurements were located between Io's M-shell and the main oval, but a few low-density measurements were found to occur near the auroral oval at low altitudes, which may be important in future particle acceleration studies. We compared our high-latitude measurements to densities obtained by whistler observations made by the Voyager 1 spacecraft and found consistent measurements, but also lower peak densities, which is expected at higher latitudes. Density gradients were observed near the inner edge of the Io torus, which was previously observed in the inner magnetosphere by the Galileo spacecraft revealing the high-latitude extension of the inner edge of the torus. More recently, observations of cold ionospheric ions and precipitating magnetospheric ions by the JADE-I sensor showed a gradient in the flux at the same location as the Waves electron density measurements (Valek et al., 2019). These observations demonstrate the extension of elevated Io torus densities along field lines to higher latitudes.

We compared our electron density measurements to partial electron densities measured by the JADE instrument and found good agreement with times when both Waves and JADE can make the measurement. There are often times of high radiation and the mean electron energy is outside the range of the JADE sensors, which is why the use of plasma wave density measurements is important because they support plasma instruments through indirect measurements of electron densities. We hope future studies can utilize our density data set as inputs for various magnetospheric plasma models. Further electron density studies covering the equatorial and Io plasma torus regions, through Juno's extended mission, will make it possible to expand our density data set and perform comparative studies with high-latitude electron densities.

Data Availability Statement

The data used in this study are publicly accessible through the Planetary Data System (https://pds.jpl.nasa.gov). The tabulated Waves densities, characteristic frequencies, and ephemeris parameters used in this study can be found at https://doi.org/10.5281/zenodo.4456343 (Author comment: this link will be finalized once the manuscript has been accepted for publication).

Acknowledgments
The research conducted at the University of Iowa was supported by NASA through contract 699041X with the Southwest Research Institute. The authors would like to thank L. Granroth for assistance in creating this site.

References

Allegrini, F., Kurth, W. S., Elliott, S. S., Saur, J., Livadiotis, G., Nicolaou, G., et al. (2021). Electron partial density and temperature over Jupiter's main auroral emission from Juno. *Journal of Geophysical Research: Space Physics*.

Allegrini, F., Mauk, B., Clark, G., Gladstone, G. R., Hue, V., Kurth, W. S., et al. (2020). Energy flux and characteristic energy of electrons over Jupiter's main auroral emission. *Journal of Geophysical Research: Space Physics*, *125*, e2019JA027693. https://doi.org/10.1029/2019ja027693

Ansher, J. A., Kurth, W. S., Gurnett, D. A., & Goertz, C. K. (1992). High resolution measurements of density structures in the Jovian plasma sheet. *Geophysical Research Letters*, *19*, 2281–2284. https://doi.org/10.1029/92GL02630

Bagenal, F. (1994). Empirical model of the Io plasma torus: Voyager measurements. *Journal of Geophysical Research*, *99*(A6), 11043–11062. https://doi.org/10.1029/93JA02908

Bagenal, F., Adriani, A., Allegrini, F., Bolton, S. J., Bonfond, B., Bunce,E. J., et al. (2017). Magnetospheric science objectives of the Juno mission. *Space Science Reviews*, 213. https://doi.org/10.1007/s11214-014-0036-8

Bagenal, F., Crary, F. J., Stewart, A. I. F., Schneider, N. M., Gurnett, D. A., Kurth, W. S., et al. (1997). Galileo measurements of plasma density in the Io torus. *Geophysical Research Letters*, *24*, 2119–2122. https://doi.org/10.1029/97GL01254

Bagenal, F., & Dols, V. (2020). The space environment of Io and Europa. *Journal of Geophysical Research: Space Physics*, *125*, e2019JA027485. https://doi.org/10.1029/2019ja027485

Bagenal, F., & Sullivan, J. D. (1981). Direct plasma measurements in the Io torus and inner magnetosphere of Jupiter. *Journal of Geophysical Research*, *86*(A10), 8447–8466. https://doi.org/10.1029/JA086iA10p08447

Bagenal, F., Sullivan, J. D., & Siscoe, G. L. (1980). Spatial distribution of plasma in the Io torus. *Geophysical Research Letters*, *7*, 41–44. https://doi.org/10.1029/GL007i001p00041

Bagenal, F., Wilson, R. J., Siler, S., Paterson, W. R., & Kurth, W. S. (2016). Survey of Galileo plasma observations in Jupiter's plasma sheet. *Journal of Geophysical Research Planets*, *121*, 871–894. https://doi.org/10.1002/2016JE005009

Barbosa, D. D., Kurth, W. S., Moses, S. L., & Scarf, F. L. (1990). *Z* mode radiation in Jupiter's magnetosphere: The source of Jovian continuum radiation. *Journal of Geophysical Research*, *95*(A6), 8187–8196. https://doi.org/10.1029/JA095iA06p08187

Barnhart, B. L., Kurth, W. S., Groene, J. B., Faden, J. B., Santolik, O., & Gurnett, D. A. (2009). Electron densities in Jupiter's outer magnetosphere determined from Voyager 1 and 2 plasma wave spectra. *Journal of Geophysical Research*, *114*(A5). https://doi.org/10.1029/2009JA014069

Birmingham, T. J., Alexander, J. K., Desch, M. D., Hubbard, R. F., & Pedersen, B. M. (1981). Observations of electron gyroharmonic waves and the structure of the Io torus. *Journal of Geophysical Research*, *86*(A10), 8497–8507. https://doi.org/10.1029/JA086iA10p08497

Bolton, S. J., Lunine, J., Stevenson, D., Connerney, J. E. P., Levin, S., Owen, T. C., et al. (2017). The Juno mission. *Space Science Reviews*, *213*, 5–37. https://doi.org/10.1007/s11214-017-0429-6

Bonfond, B., Gladstone, G. R., Grodent, D., Greathouse, T. K., Versteeg, M. H., Hue, V., et al. (2017). Morphology of the UV aurorae Jupiter during Juno's first perijove observations. *Geophysical Research Letters*, *44*, 4463–4471. https://doi.org/10.1002/2017GL073114

Bonfond, B., Grodent, D., Gérard, J.-C., Stallard, T., Clarke, J. T., Yoneda, M., et al. (2012). Auroral evidence of Io's control over the magnetosphere of Jupiter. *Geophysical Research Letters*, *39*, L01105. https://doi.org/10.1029/2011GL050253

Brown, R. A. (1976). A model of Jupiter' s sulfur nebula. *The Astrophysical Journal*, *206*, LI79–L183. https://doi.org/10.1086/182162

Connerney, J. E. P., Acuna, M. H., & Ness, N. F. (1981). Modeling the Jovian current sheet and inner magnetosphere. *Journal of Geophysical Research*, *86*. https://doi.org/10.1029/JA086iA10p08370

Connerney, J. E. P., Benn, M., Bjarno, J. B., Denver, T., Espley, J., Jorgensen, J. L., et al. (2017). The Juno magnetic field investigation. *Space Science Reviews*, *328*, 213. https://doi.org/10.1007/s11214-017-0334-z329

Connerney, J. E. P., Kotsiaros, S., Oliversen, R. J., Espley, J. R., Joergensen, J. L., Joergensen, P. S., et al. (2018). A new model of Jupiter's magnetic field from Juno's first nine 330 orbits. *Geophysical Research Letters*, *45*, 2590–2596. https://doi.org/10.1002/2018GL077312

Crary, F. J., Bagenal, F., Ansher, J. A., Gurnett, D. A., & Kurth, W. S. (1996). Anisotropy and proton density in the Io plasma torus derived from whistler wave dispersion. *Journal of Geophysical Research*, *101*(A2), 2699–2706. https://doi.org/10.1029/95JA02212

Gurnett, D. A., & Bhattacharjee, A. (2017). *Introduction to plasma physics: With space and laboratory applications*. Cambridge University Press.

Gurnett, D. A., & Frank, L. A. (1974). Thermal and suprathermal plasma densities in the outer magnetosphere. *Journal of Geophysical Research*, *79*(16), 2355–2361. https://doi.org/10.1029/JA079i016p02355

Gurnett, D. A., Kurth, W. S., Roux, A., Bolton, S. J., & Kennel, C. F. (1996). Galileo plasma wave observations in the Io plasma torus and near Io. *Science*, *274*, 391–392. https://doi.org/10.1126/science.274.5286.391

Gurnett, D. A., Kurth, W. S., Roux, A., Bolton, S. J., Thomsen, E. A., & Green, J. B. (1998). Galileo plasma wave observations near Europa. *Geophysical Research Letters*, *25*, 237–240. https://doi.org/10.1029/97GL03706

Gurnett, D. A., Kurth, W. S., & Scarf, F. L. (1979). Plasma wave observations near Jupiter: Initial results from Voyager 2. *Science*, *206*, 987–991. https://doi.org/10.1126/science.206.4421.987

Gurnett, D. A., Kurth, W. S., & Scarf, F. L. (1980). The structure of the Jovian magnetotail from plasma wave observations. *Geophysical Research Letters*, *7*, 53–56. https://doi.org/10.1029/GL007i001p00053

Gurnett, D. A., Persoon, A. M., Kurth, W. S., Roux, A., & Bolton, S. J. (2001). Electron densities near Io from Galileo plasma wave observations. *Journal of Geophysical Research*, *106*(A11), 26225–26232. https://doi.org/10.1029/2000JA002509

Gurnett, D. A., Scarf, F. L., Kurth, W. S., Shaw, R. R., & Poynter, R. L. (1981). Determination of Jupiter's electron density profile from plasma wave observations. *Journal of Geophysical Research*, *86*(A10), 8199–8212. https://doi.org/10.1029/JA086iA10p08199

Gurnett, D. A., & Shaw, R. R. (1973). Electromagnetic radiation trapped in the magnetosphere above the plasma frequency. *Journal of Geophysical Research*, *78*(34), 8136–8149. https://doi.org/10.1029/JA078i034p08136

Hess, S. L. G., Bonfond, B., Chantry, V., Gérard, J.-C., Grodent, D., Jacobsen, S., & Radioti, A. (2013). Evolution of the Io footprint brightness II: Modeling. *Planatary Space Science*, *88*, 76–85. https://doi.org/10.1016/j.pss.2013.08.005

Kupo, I., Mekler, Y., & Eviatar, A. (1976). Detection of ionized sulphur in the Jovian magnetosphere. *Astrophysical Journal*, *205*, L51–L54. https://doi.org/10.1086/182088

Kurth, W., Craven, J., Frank, L., & Gurnett, D. (1979). Intense electrostatic waves near the upper hybrid resonance frequency. *Journal of Geophysical Research*, *84*(A8), 4145–4164. https://doi.org/10.1029/JA084iA08p04145

Kurth, W. S., Barbosa, D. D., Gurnett, D. A., & Scarf, F. L. (1980). Electrostatic waves in the Jovian magnetosphere. *Geophysical Research Letters*, *7*, 57–60. https://doi.org/10.1029/GL007i001p00057

Kurth, W. S., De Pascuale, S., Faden, J. B., Kletzing, C. A., Hospodarsky, G. B., Thaller, S., & Wygant, J. R. (2015). Electron densities inferred from plasma wave spectra obtained by the waves instrument on Van Allen Probes. *Journal of Geophysical Research Space Physics*, *120*, 904–914. https://doi.org/10.1002/2014JA020857

Kurth, W. S., Hospodarsky, G. B., Kirchner, D. L., Mokrzycki, B. T., Averkamp, T. F., Robison, W. T., et al. (2017). The Juno waves investigation. *Space Science Reviews*, *213*, 347–392. https://doi.org/10.1007/s11214-017-0396-y

Le Chat, G., Issautier, K., Meyer-Vernet, N., Zouganelis, I., Maksimovic, M., & Moncuquet, M. (2009). Quasi-thermal noise in space plasma: "Kappa" distributions. *Physics of Plasmas*, *16*, 102903. https://doi.org/10.1063/1.3243495

Lysak, R. L., & Song, Y. (2011). Development of parallel electric fields at the plasma sheet boundary layer. *Journal of Geophysical Research*, *116*, A00K14. https://doi.org/10.1029/2010JA016424

McComas, D. J., Alexander, N., Allegrini, F., Bagenal, F., Beebe, C., Clark, G., et al. (2017). The Jovian auroral distributions experiment (JADE) on the Juno mission to Jupiter. *Space Science Reviews*, *213*, 547–643. https://doi.org/10.1007/s11214-013-9990-9

Menietti, J. D., Gurnett, D. A., & Groene, J. B. (2005). Radio emission observed by Galileo in the inner Jovian magnetosphere during orbit A-34. *Planetary and Space Science*, *53*, 1234–1242. https://doi.org/10.1016/j.pss.2005.06.001

Meyer-Vernet, N., & Perche, C. (1989). Tool kit for antennae and thermal noise near the plasma frequency. *Journal of Geophysical Research*, *94*(A3), 2405–2415. https://doi.org/10.1029/JA094iA03p02405

Moncuquet, M., Bagenal, F., & Meyer-Vernet, N. (2002). Latitudinal structure of outer Io plasma torus. *Journal of Geophysical Research*, *107*(A9), 1260. https://doi.org/10.1029/2001JA900124

Mosier, S. R., Kaiser, M. L., & Brown, L. W. (1973). Observations of noise bands associated with the upper hybrid resonance by the Imp 6 radio astronomy experiment. *Journal of Geophysical Research*, *78*(10), 1673–1679. https://doi.org/10.1029/JA078i010p01673

Paschmann, G., Haaland, S., & Treumann, R. (Eds). (2003). *Auroral plasma physics*. Kluwer Acad.

Persoon, A. M., Gurnett, D. A., Kurth, W. S., Hospodarsky, G. B., Groene, J. B., Canu, P., & Dougherty, M. K. (2005). Equatorial electron density measurements in Saturn's inner magnetosphere. *Geophysical Research Letters*, *32*, L23105. https://doi.org/10.1029/2005GL024294

Persoon, A. M., Gurnett, D. A., Peterson, W. K., Waite, J. H., Jr., Burch, J. L., & Green, J. L. (1988). Electron density depletions in the nightside auroral zone. *Journal of Geophysical Research*, *93*, 1871–1895. https://doi.org/10.1029/JA093iA03p0187

Persoon, A. M., Kurth, W. S., Gurnett, D. A., Groene, J. B., Sulaiman, A. H., Wahlund, J.-E., et al. (2019). Electron density distributions in Saturn's ionosphere. *Geophysical Research Letters*, *46*, 3061–3068. https://doi.org/10.1029/2018gl078020

Russell, C. T. (2004). Outer planet magnetospheres: A tutorial. *Advances in Space Research*, *33*, 2004–2020. https://doi.org/10.1016/j.asr.2003.04.049

Russell, C. T. (2006). New horizons in planetary magnetospheres. *Advances in Space Research*, *37*, 1467–1481. https://doi.org/10.1016/j.asr.2005.03.133

Scarf, F. L., Gurnett, D. A., & Kurth, W. S. (1979). Jupiter plasma wave observations: An initial Voyager 1 overview. *Science*, *204*, 991–995. https://doi.org/10.1126/science.204.4396.991

Scudder, J. D., Sittler, E. C., & Bridge, H. S. (1981). A survey of the plasma electron environment of Jupiter: A view from Voyager. *Journal of Geophysical Research*, *86*, 8157–8179. https://doi.org/10.1029/JA086iA10p08157

Shaw, R. R., & Gurnett, D. A. (1975). Electrostatic noise bands associated with the electron gyrofrequency and plasma frequency in the outer magnetosphere. *Journal of Geophysical Research*, *80*(31), 4259–4271. https://doi.org/10.1029/JA080i031p04259

Sittler, E. C., & Strobel, D. F. (1987). Io plasma torus electrons: Voyager 1. *Journal of Geophysical Research*, *92*(A6), 5741–5762. https://doi.org/10.1029/JA092iA06p05741

Stix, T. H. (1962). *The theory of plasma waves*. McGraw-Hill.

Sulaiman, A. H., Elliott, S. S., Kurth, W. S., Faden, J. B., & Hospodarsky, G. B. (2021). Inferring Jovian electron densities using plasma wave spectra obtained by the Juno/Waves instrument. *Journal of Geophysical Research: Space Physics*. https://doi.org/10.1029/2021JA029263

Sulaiman, A. H., Hospodarsky, G. B., Elliott, S. S., Kurth, W. S., Gurnett, D. A., Imai, M., et al. (2020). Wave-particle interactions associated with Io's auroral footprint: Evidence of Alfvén, ion cyclotron, and whistler modes. *Geophysical Research Letters*, *47*, e2020GL088432. https://doi.org/10.1029/2020gl088432

Sulaiman, A. H., Kurth, W. S., Persoon, A. M., Menietti, J. D., Farrell, W. M., Ye, S. Y., et al. (2017). Intense harmonic emissions observed in Saturn's ionosphere. *Geophysical Research Letters*, *44*, 24. https://doi.org/10.1002/2017GL076184

Szalay, J. R., Allegrini, F., Bagenal, F., Bolton, S. J., Bonfond, B., Clark, G., et al. (2020). A new framework to explain changes in Io's footprint tail electron fluxes. *Geophysical Research Letters*, *47*, e2020GL089267. https://doi.org/10.1029/2020gl089267

Szalay, J. R., Allegrini, F., Bagenal, F., Bolton, S. J., Clark, G., Connerney, J. E. P., et al. (2021). Proton outflow associated with Jupiter's auroral processes. *Geophysical Research Letters*, *48*, e2020GL091627. https://doi.org/10.1029/2020gl091627

Thomas, N., Bagenal, F., Hill, T., & Wilson, J. (2004). The Io neutral clouds and plasma torus. In F. Bagenal, T. E. Dowling, & W. B. McKinnon (Eds.), *Jupiter: Planet, satellites, magnetosphere*. Cambridge University Press.

Tokar, R. L., Gurnett, D. A., Bagenal, F., & Shaw, R. R. (1982). Light ion concentrations in Jupiter's inner magnetosphere. *Journal of Geophysical Research*, *87*(A4), 2241–2245. https://doi.org/10.1029/JA087iA04p02241

Valek, P. W., Allegrini, F., Bagenal, F., Bolton, S. J., Connerney, J. E. P., Ebert, R. W., et al. (2019). Jovian high-latitude ionospheric ions: Juno in situ observations. *Geophysical Research Letters*, *46*, 8663–8670. https://doi.org/10.1029/2019GL084146

Wang, K., Thorne, R. M., Home, R. B., & Kurth, W. S. (1998a). Constraints on Jovian plasma properties from a dispersion analysis of unducted whistlers in the warm Io torus. *Journal of Geophysical Research*, *103*(A7), 14979–14986. https://doi.org/10.1029/98JA00964

Wang, K., Thorne, R. M., Home, R. B., & Kurth, W. S. (1998b). Cold torus whistlers: An indirect probe of the inner Jovian plasmasphere. *Journal of Geophysical Research*, *103*(A7), 14987–14994. https://doi.org/10.1029/98JA00965

Warwick, J. W., Pearce, J. B., Riddle, A. C., Alexander, J. K., Desch, M. D., Kaiser, M. L., et al. (1979). Voyager 1 planetary radio astronomy observations near Jupiter. *Science*, *204*, 995–998. https://doi.org/10.1126/science.204.4396.995